TABLE I. Laser emission wavelengths.

$\lambda_{(vac)}$ (μ)	τ_s (μsec)	τ_D (μsec)	Intensity	Resonator configuration[b]
14.78	5	3	strong	a,c
15.04	3	2	weak	a,
15.08	5	3	weak	a,c
15.41	3	2	weak	a,
15.47	5	4	strong	a,c
18.21	2	3	medium	b,c
21.46[a]	3	3	medium	a,b,c
22.54[a]	2	4	strong	a,b,c
22.71	4	4	strong	a,b,c
23.68[a]	2	5	strong	a,b,c
23.86	3	6	strong	a,b,c
24.92[a]	2	5	strong	a,b,c
25.12	5	6	strong	a,b,c
26.27[a]	4	3	strong	a,b,c
30.69	3	3	weak	a,c
31.47	5	2	weak	a
31.92[a]	2	4	strong	a,b,c
32.13	5	6	strong	a,b,c

[a] These lines observed by Mathias *et al.*

[b] Resonator configuration: a, non-frequency selective; b, frequency selective, 22 μ grating; c, frequency selective, 30 μ grating. Error in wavelength is $\pm 0.03\ \mu$ for $\lambda > 20\ \mu$, $\pm 0.02\ \mu$ for $\lambda < 20\ \mu$.

seven emission lines between 21 and 32 μ. In the present experiment a total of 18 lines have been observed, of which 12 have not been previously reported.

The general laser set up has been described previously.[2] The mirrors, one flat and one 15 m radius, are aluminized and spaced 4.9 m inside a 10 cm diam discharge tube. Power is coupled out a 2 mm hole in the curved mirror and passes through a high-density polyethylene vacuum window. The 5C22 modulator used produces current pulses of 4 μsec duration and peak currents of 500–600 A (at voltages from 6–8 kV) with rise- and falltimes of the order of 0.5 μsec. The laser emission was observed at pulse repetition rates of 1–5 pps. The ammonia (obtained from Matheson Co.) was pumped with a 250 liter/min forepump at an average pressure of 0.5–1.0 Torr.

The laser emission was detected with Ga:Ge and Cu:Ge detectors cooled to 4°K and the wavelengths measured with a 0.5 m Bausch & Lomb monochromator using gratings blased for 22.5 and 9 μ.

The laser was also operated in a frequency-selective mode by replacing the flat mirror with gratings blased at 22 and 30 μ. This produced one new line at 18.21 μ, which apparently is in competition with one or more of the other emission lines.

Table I gives a list of all observed lines together with the starting time (τ_s), measured from the beginning of the 4 μsec current pulse, and the emission duration (τ_d). A very rough indication of intensity is given where "strong" is used to indicate that the detector is saturated when the monochromator slits are opened wide enough to observe the "weak" lines.

The authors acknowledge helpful discussions with Dr. John Hassler.

* This research was supported by the Electronics Division of the Air Force Office of Scientific Research.

[1] L. E. S. Mathias, A. Crocker, and M. S. Wills, Phys. Letters **14**, 33 (1965).

[2] D. P. Akitt, W. Q. Jeffers, and P. D. Coleman, Proc. IEEE **54**, 547 (1965).

Mobility of Dislocations in Aluminum at 74° and 83°K*

J. A. GORMAN, D. S. WOOD, AND T. VREELAND, JR.
W. M. Keck Laboratories, California Institute of Technology, Pasadena, California 91109
(Received 2 October 1968)

In a previous article[1] the authors reported determinations of the velocity of dislocations in high-purity single crystals of aluminum as a function of applied stress in the temperature range 123° to 343°K. These results were obtained using a stress-pulse technique in which dislocation positions were observed before and after the stress pulse using the Berg–Barrett x-ray technique. This note reports an extension of the dislocation velocity measurements in aluminum to lower temperatures, 74° and 83°K, and discusses their significance.

Dislocation velocities at 74° and 83°K were obtained by the method described previously,[1] except that the aluminum single-crystal test specimens were bonded to the torsion-stress pulse machine using mixtures of isopentane and methylcyclohexane, which form glasses at temperatures slightly below the test temperatures. The dislocation velocity data obtained at 74° and 83°K are shown as functions of the applied-resolved shear stress in Fig. 1. The dashed lines in Fig. 1 are straight lines from the origin to a point obtained by averaging all the stress-velocity data for the given temperature.

The dislocation drag coefficient, which is the ratio of the drag force acting on a unit length of dislocation to the dislocation velocity, was obtained from the stress-velocity data as described previously.[1] The values obtained were 1.33×10^{-4} dyne-sec/cm^2 at 74°K and 1.31×10^{-4} dyne-sec/cm^2 at 83°K. These values, together with the values reported previously for higher temperatures, are plotted as circles in Fig. 2. Figure 2 also shows dislocation drag coefficients for aluminum obtained by Mason and Rosenberg[2] from ultrasonic attenuation measurements (indicated by +), and from the phonon viscosity[3,4] and electron viscosity[5,6] theories (indicated by dashed line). The experimental drag coefficients from Mason and Rosenberg and the theoretical values from the phonon and electron viscosity theories are plotted to a different scale than the present results to facilitate comparison of their temperature dependencies.

For temperatures greater than 150°K, Fig. 2 shows that the magnitude of the dislocation drag coefficient obtained by the present authors is considerably less than that obtained by Mason and Rosenberg by ultrasonic measurements and by the phonon viscosity theory, but that the temperature dependencies agree rather well. In the authors' previous paper,[1] possible reasons for the differences in the magnitude of the dislocation drag coefficient were discussed and will not be repeated here. It was concluded that the agreement in the temperature dependence tended to support the phonon viscosity theory.

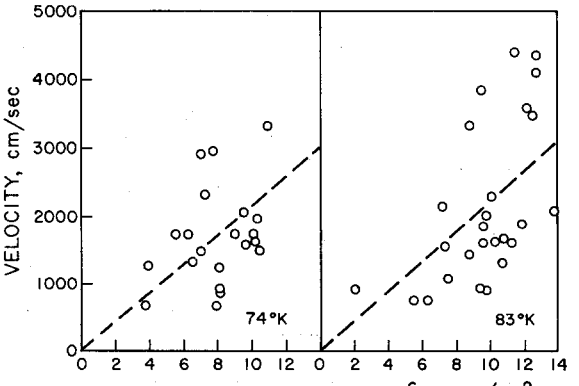

FIG. 1. Dislocation velocity vs resolved shear stress.

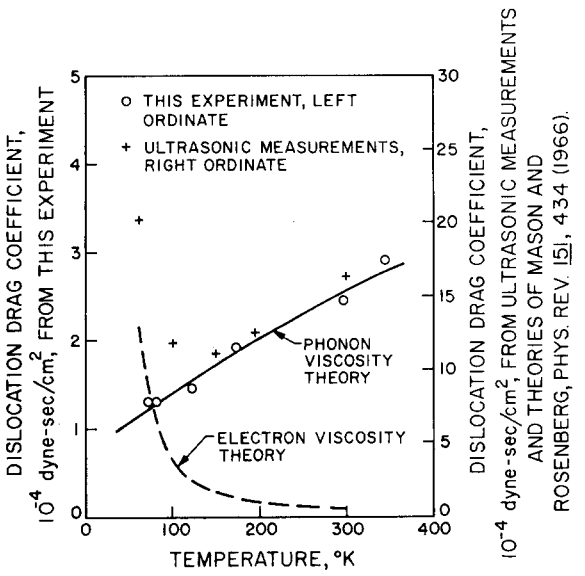

FIG. 2. Dislocation drag coefficient vs temperature.

The temperature dependence of the dislocation drag coefficient obtained by the present authors in the range 74° to 150°K does not exhibit the increase with decreasing temperature which is shown by Mason and Rosenberg's experimental and theoretically predicted results.

The present results thus indicate, in contrast to Mason and Rosenberg, that in aluminum the dislocation drag due to electron viscosity is negligible compared to the phonon drag for temperatures greater than 74°K. Further direct velocity measurements at temperatures below 74°K are needed to establish the importance of electron viscosity in aluminum.[5]

* This work was supported by the U. S. Atomic Energy Commission.

[1] J. A. Gorman, D. S. Wood, and T. Vreeland, Jr., J. Appl. Phys. **40**, 833 (1969), this issue.

[2] W. P. Mason and A. Rosenberg, Phys. Rev. **151**, 434 (1966).

[3] W. P. Mason, J. Acoust. Soc. Am. **32**, 458 (1960).

[4] W. P. Mason, J. Appl. Phys. **35**, 2779 (1964).

[5] W. P. Mason, *Physical Acoustics and the Properties of Solids* (D. Van Nostrand Co., Inc., Princeton, N. J., 1958), p. 323.

[6] W. P. Mason, Appl. Phys. Letters **6**, 111 (1965).

Quenched Bulk GaAs Oscillators with Doping Gradients

H. W. THIM AND K. KUROKAWA

Bell Telephone Laboratories, Incorporated, Murray Hill, New Jersey 07974

(Received 27 September 1968)

In a recent paper,[1] it was shown that multiple dipoles could form in one-dimensional bulk GaAs oscillators ($n_0 \times L > 10^{12}$ cm^{-2}) with microscopic random doping fluctuations, especially when operated at frequencies higher than the transit-time frequency. To supplement the above paper, this letter presents computer simulations of one-dimensional bulk GaAs oscillators with systematic (linearly increasing, linearly decreasing, concave, and convex) doping variations. Superposition of random fluctuations on top of these types of variations should give a realistic model of bulk GaAs diodes available with the present material technology.

For the first set of calculations (Figs. 1–4), the lowest donor density n_0 in the sample times the sample length L was chosen to be sufficiently large to allow dipole formation, as indicated in the figure caption, while the frequency and the load condition were adjusted to optimize the dc to rf conversion efficiency. (For lower $n_0 \times L$ product the accumulation layer mode takes place.)

The donor density in the diode of Fig. 1 has a constant slope of 10% rising from the cathode toward the anode, as shown at the lower left. The maximum efficiency of 10% was calculated with a bias voltage of $3V_T$ and a load resistance of $30R_0$ (V_T= threshold voltage, R_0=low-field resistance of the sample). The accumulation layer injected from the cathode moves only a short distance at the velocity of the conduction electrons ($\sim 1.5 \times 10^7$ cm/sec), but depletion-layer moves in from the anode toward the cathode with a velocity of about 10^8 cm/sec.

Another way of describing the space-charge dynamics is that an accumulation layer grows during the first half of the rf cycle and converts to a wide dipole which shrinks during the second half because of the falling sinusoidal voltage. The time the dipole takes to readjust can be calculated by using two successive field plots in Fig. 1. The elasped time between plots 2 and 3 is only 10 psec. The rate of change of excess voltage (voltage under the dipole area) is about 10^{12} V/sec, which is the maximum theoretical value obtained from the "unequal-area rule."[2] However, the external voltage changes at a rate of 5×10^{12} V/sec. The dipole is easily quenched because its capacitance and the positive resistance outside the dipole are small. When the slope of the doping gradient was increased to 50%, the field near the anode remained below the threshold value resulting in a lower efficiency of 5.5% ($R_L = 70R_0$, $V_B = 3V_T$). When the doping gradient was

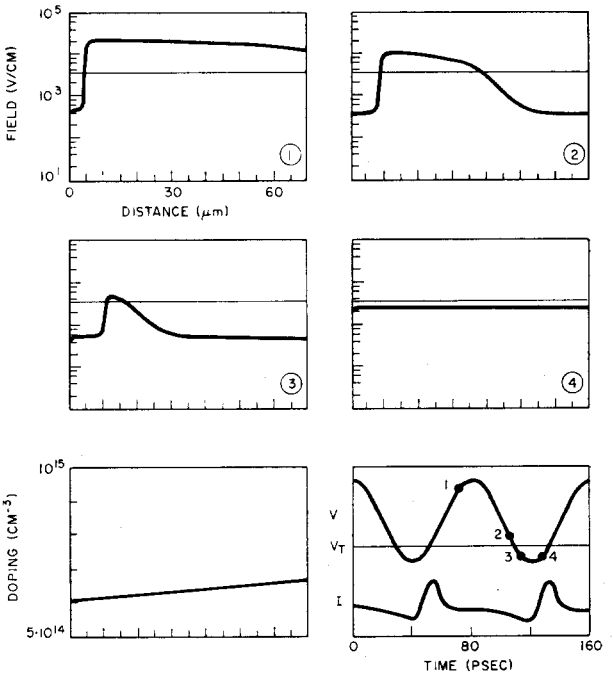

FIG. 1. The upper 4 plots show the electric field vs distance at four different times during one rf cycle. The numbers 1–4 in the lower-right corners correspond to the different times shown on the rf voltage waveform at the bottom right. The straight horizontal lines in the upper 4 plots represent the threshold field (3800 V/cm). The GaAs electronic current vs time is shown beneath the voltage waveform. The left picture on the bottom shows the doping profile (10% gradient rising toward anode). Parameters used in all calculations (Figs. 1–4) are:

$n_0 = 6 \times 10^{14}$ cm^{-3} $\quad n_0 \times L = 4.2 \times 10^{12}$ cm^{-2}

$L = 70\ \mu$ or $f \times L = 8.4 \times 10^7$ cm/sec

$f = 12$ GHz $\quad n_0/f = 5 \times 10^4$ cm^{-3}·sec.

The velocity-field characteristic is the same as that used in Ref. 1.